Title Page

Characterization of molecular mechanisms underlying the axonal Charcot-Marie-Tooth neuropathy caused by *MORC2* mutations

Paula Sancho[1¶], Luca Bartesaghi[2,3¶], Olivia Miossec[2,3], Francisco García-García[4], Laura Ramírez-Jiménez[5], Anna Siddell[6,7], Elisabet Åkesson[8,9], Eva Hedlund[2], Petra Laššuthová[10], Samuel I. Pascual-Pascual[11], Teresa Sevilla[12,13], Marina Kennerson[6,7,14], Vincenzo Lupo[1,5,15&], Roman Chrast[2,3&*], Carmen Espinós[1,5,15&*]

[1] Unit of Genetics and Genomics of Neuromuscular and Neurodegenerative Disorders, Centro de Investigación Príncipe Felipe (CIPF), 46012 Valencia, Spain

[2] Department of Neuroscience, Karolinska Institutet, 17165 Stockholm, Sweden

[3] Department of Clinical Neuroscience, Karolinska Institutet, 17165 Stockholm, Sweden

[4] Unit of Bioinformatics and Biostatistics, Centro de Investigación Príncipe Felipe (CIPF), 46012 Valencia, Spain

[5] Department of Genomics and Translational Genetics, Centro de Investigación Príncipe Felipe (CIPF), 46012 Valencia, Spain

[6] Northcott Neuroscience Laboratory, ANZAC Research Institute, Concord NSW 2139, Australia

[7] Sydney Medical School, University of Sydney, Sydney NSW 2006, Australia

[8] Division of Neurodegeneration, Department of Neurobiology, Care Sciences and Society, Karolinska Institutet, 14152 Stockholm, Sweden

[9] The R&D Unit, Stiftelsen Stockholms Sjukhemm, 14152 Stockholm, Sweden

[10] Department of Pediatric Neurology, DNA Laboratory, 2nd Faculty of Medicine, Charles University in Prague and University Hospital Motol, 15006 Prague, Czech Republic

[11] Department of Pediatric Neurology, Hospital Universitario La Paz, 28046 Madrid, Spain

[12] Department of Neurology, Hospital Universitari i Politècnic La Fe, and CIBER of Rare Diseases (CIBERER), 46026 Valencia, Spain

[13] Department of Medicine, University of Valencia, 46010 Valencia, Spain

[14] Molecular Medicine Laboratory, Concord Hospital, Concord NSW 2139, Australia

[15] INCLIVA & IIS-La Fe Rare Diseases Joint Units, Centro de Investigación Príncipe Felipe (CIPF), 46012 Valencia, Spain

[¶]These authors contributed equally to this work.

[&]These authors also contributed equally to this work.

*Co-corresponding authors:

Carmen Espinós. Department of Genomics and Translational Genetics, Centro de Investigación Príncipe Felipe (CIPF), 46012 Valencia, Spain. Tel. +34-963289680; Fax: +34-963289701; Email: cespinos@cipf.es.

Roman Chrast. Department of Neuroscience, Karolinska Institutet, 17165 Stockholm, Sweden. Tel. +46-852487825; Fax: +46-8311101; Email: roman.chrast@ki.se.

ABSTRACT

Mutations in *MORC2* lead to an axonal form of Charcot-Marie-Tooth neuropathy (CMT) type 2Z. To date, thirty-one families have been described with mutations in *MORC2*, indicating that this gene is frequently involved in axonal CMT cases. While the genetic data clearly establishes the causative role of *MORC2* in CMT2Z, the impact of its mutations on neuronal biology and their phenotypic consequences in patients remains to be clarified. We show that the full-length form of MORC2 is highly expressed in both embryonic and adult human neural tissues and that Morc2 expression is dynamically regulated in both the developing and the maturing murine nervous system. To determine the effect of the most common MORC2 mutations, p.S87L and p.R252W, we used several *in vitro* cell culture paradigms. Both mutations induced transcriptional changes in patient-derived fibroblasts and when expressed in rodent sensory neurons. These changes were more pronounced, and accompanied by abnormal axonal morphology, in neurons expressing the MORC2 p.S87L mutation, which is associated with a more severe clinical phenotype. These data provide insight into the neuronal specificity of the mutated MORC2-mediated phenotype and highlight the importance of neuronal cell models to study the pathophysiology of CMT2Z.

INTRODUCTION

Charcot-Marie-Tooth (CMT) disease is the most frequently inherited neurological disease with a prevalence of 28/100,000, and refers to a clinically heterogeneous demyelinating or axonal neuropathy that affects peripheral nerves (1-3). More than 80 genes have been linked to different forms of CMT (Neuromuscular Disease Center; http://neuromuscular.wustl.edu/time/hmsn.html). As a part of our ongoing effort to identify new genes implicated in CMT, we recently detected a novel variant c.568C>T (p.R190W) in *MORC2* in an axonal CMT family [4]. The mutational screening of *MORC2* in available clinical cohorts allowed the diagnosis of two additional sporadic cases: one with the same mutation and the other with a novel missense mutation c.74C>T (p.S25L) (4). The c.568C>T (p.R190W) and the c.74C>T (p.S25L) mutations are also named c.754C>T (p.R252W) and c.260C>T (p.S87L), based on the isoform encoding the NM_001303256 MORC2 transcript (5).

Currently, thirty-one families have been identified with mutations in *MORC2*, showing its frequent implication in CMT in various populations (4-13). This new form of axonal CMT (CMT2Z; MIM 616688) presents with a number of both early and late onset heterogeneous clinical features, including a spinal muscular atrophy (SMA) phenotype, axonal neuropathy with pyramidal signs, distal and proximal weakness in an asymmetric and random manner associated with important sensory loss, and the appearance of cerebellar atrophy and diaphragmatic paralysis. The most frequent mutation is the p.R252W which represents more than 50% of cases (4-13).

Microrchidia (MORC) family CW-type zinc finger 2 (MORC2) is a member of the MORC protein family (14, 15) conserved in higher eukaryotes. Four MORC proteins have been predicted in humans that share multiple conserved domains: a GHL (Gyrase B, Hsp90, and MutL)-ATPase domain at the amino-terminus, a CW-type zinc

finger domain, and three predicted coiled-coil domains. Several functions have been attributed to MORC2: gene transcriptional repression in gastric cancer cells (16); promotion of breast cancer invasion and metastasis (17); interaction with ATP-citrate lyase (ACLY), involvement in lipogenesis and adipogenesis (18); transcriptional regulation of ArgBP2, which is part of actin-dependent processes such as cell adhesion and migration (19); and as substrate of PAK1 (p21-activated kinase 1), an integrator of extracellular signals and nuclear processes (20). Importantly, MORC2 also functions as an effector of epigenetic silencing by the HUSH (human silencing hub) complex (21). Dimerization and DNA binding of the MORC2 ATPase module was shown to be implicated in HUSH-mediated repression (22).

In this study, the characterization of MORC2 expression reveals its dynamic regulation in the developing and mature peripheral and central nervous systems. To investigate the pathophysiological mechanism underlying neurodegeneration caused by *MORC2* mutations, various cellular models, including HeLa cells, patient-derived fibroblasts and primary neuronal cultures, have been used. Our data indicate that while *MORC2* mutations result in transcriptional changes in non-neuronal cells, the pathogenic phenotype is more pronounced in neurons, where detectable axonal alterations were observed. These data provide insight into the neuronal specificity of the MORC2 mediated disease phenotype and highlights the importance of neuronal-based cellular models to study the pathophysiology of CMT2Z.

RESULTS

Analysis of the expression of MORC2 isoforms in human nervous tissues

The human *MORC2* gene is transcribed as two transcripts: NM_001303256 (4,469 bp) encoding a 1,032 aa protein (NP_001290186) and the NM_014941 (5,181 bp) encoding

a protein of 970 aa (NP_055756). Due to the presence of an additional exon containing several STOP codons, the translation of the longer transcript (NM_014941) is initiated at an in-frame downstream start codon resulting in the shorter 970 aa protein (NP_055756; Fig 1A). The two mutations presented in this manuscript can therefore be named p.S25L and p.R190W based on the short protein isoform (NP_055756, 970 aa), or p.S87L and p.R252W based on the long protein isoform (NP_01290186, 1032 aa) (Fig. 1A).

To establish which *MORC2* isoform is present in human nervous tissues, we used a real time-PCR (RT-PCR) based approach. Three specific primer pairs were designed to amplify cDNA templates prepared from human dorsal root ganglia (DRG) collected at different developmental stages and from adult spinal cord. Using primer pairs hMORC2_1F/R and hMORC2_2F/R, we detected a 155 bp and a 114 bp amplicons, which both correspond to NM_001303256 encoding the longer (1,032 aa) MORC2 protein (Fig. 1A and B). The lack of amplification of the 1,021 bp amplicon with the hMORC2_1F/R primers indicate that the NM_001303256 transcript is predominantly expressed in the first trimester embryonic and adult human neural tissues. This observation was confirmed by using hMORC2_3F/R primers specific for the NM_014941 transcript encoding the 970 aa protein isoform. PCR amplification did not detect the expected 131 bp amplicon in spinal cord samples and only very weak expression of this amplicon was observed in the DRG tissue (Fig. 1A and B). Similar results were obtained using the human neuronal and non-neuronal cell lines SH-SY5Y and HEK-293T respectively (Supplementary Material, Fig. S1). Together, these data demonstrate that the transcript NM_001303256 encoding the long (1,032 aa) isoform of the MORC2 protein is the predominant form expressed in neural tissues.

Spatiotemporal expression profile of *Morc2* in mice

qPCR (quantitative PCR)-based profiling revealed that *Morc2* is dynamically regulated in brain with a peak in expression at E17.5 to P2 followed by lower levels of expression at P10 and during adulthood (Fig. 2A and B). A substantial developmental decrease was also observed in the spinal cord and in sciatic nerve. Additionally, *Morc2* was expressed in E17.5 DRG as well as in primary cultures of Schwann cells and DRG sensory neurons (Fig. 2A and B). Western-blot analysis using samples from brain and sciatic nerves revealed a similar protein expression profile to the mRNA analysis. Morc2 protein showed peak expression at the earlier stages with a progressive decrease during aging (Fig. 2C and D).

Molecular pathomechanism of the *MORC2* mutations

Since we identified the first two *MORC2* mutations in three unrelated CMT2Z families (4), a total of thirty-one families have now been reported (5-13).Our ongoing characterization of CMT patients, identified two additional CMT2Z families, one carrying the p.R252W mutation and another one with a novel missense variant c.1217C>T (p.A406V) (23). Taking into account the known thirty-three CMT2Z families, the most frequent mutation is p.R252W (17 cases; 51.5% of CMT2Z cases) (Fig. 3A). In 15 out of the 17 families with the p.R252W mutation, the mutational event occurred *de novo*. The cytosine nucleotide (c.754C) involved with the p.R252W mutation is located in a CpG dinucleotide. Using sodium bisulphite sequencing of control DNA, 5mC cytosine nucleotides were identified in genomic DNA surrounding the c.C754T change. Primers were designed to amplify a 278 bp amplicon containing the c.754C nucleotide. A total of 15 cytosines were identified and analysed in the amplicon with > 99% of the non-CpG dinucleotide cytosines being converted to

thymidine reflecting their unmethylated status (Fig. 3B). In contrast, the cytosines located in CpG dinucleotides were mostly unconverted (Fig. 3B). In particular, the cytosine nucleotide giving rise to the p.R252W was unconverted to thymidine in 12 of the 19 bisulphite-treated DNA clones assessed indicating the predominantly methylated status of c.754C potentially contributing to its behavior as a mutational hotspot (Fig. 3B).

To date, the ten different MORC2 mutations are known to be located in the ATPase domain (p.S87L, p.R132L, p.E236G and p.R252W), or next to this domain, in a transition position between the first coiled-coil and the CW-type finger domain (p.Q400R, p.C407Y, p.A431V, p.T424R, p.D466N and p.A406V) with relative homology with the ribosomal S5 domain (21) (Fig. 4A). A more detailed analysis was undertaken on p.R252W, which is the most frequent mutation, and on p.S87L, which is reported to be associated with the most severe CMT2Z phenotype (4). Since both mutations are located in the ATPase domain of the MORC2 protein, we first evaluated if these mutations altered ATPase activity. Western-blot analysis was used to confirm the stability of overexpressed wild-type (WT) and mutated MORC2 in HeLa cells (Fig. 4B). A colorimetric ATPase assay performed in transiently transfected HeLa cells showed that the p.S87L caused a significant reduction of the ATPase activity when compared to WT activity, while the p.R252W mutation did not (Fig. 4C).

MORC2 is known to promote the phosphorylation and activity of ACLY an enzyme involved in the formation of acetyl-coA in the cytoplasm (18). Acetyl-coA is a substrate for choline acetyl transferase, an enzyme involved in the production of acetylcholine which is a key molecule for neuronal function and survival (24). As the ATPase activity was not affected by the p.R252W mutation we evaluated if the most common mutation could affect ACLY activity, by using a previously described malate

dehydrogenase (MDH) enzyme activity assay to indirectly assess ACLY activity (25). However, the assay showed that there was no difference in MDH enzyme activity between patient p.R252W and control fibroblasts (Supplementary Material, Fig. S2).

Characterization of human fibroblasts derived from CMT2Z patients

To date, expression of MORC2 has been described mainly in the nucleus, where the majority of the MORC2 functions have been reported, and to a lesser extent, in the cytoplasm (18). By immunofluorescence analysis of control and CMT2Z patient skin biopsy-derived fibroblasts, we confirmed the previously described location for MORC2 in the nucleus and cytoplasm (Fig. 5A). Neither the p.R252W or p.S87L mutations showed an altered pattern of cellular localization. Similar findings were obtained using transfected HeLa cells (Supplementary Material, Fig. S3).

Since MORC2 was previously characterized as a transcriptional regulator (21), transcriptome analysis was used to evaluate changes in the mRNA profile of fibroblasts derived from patients carrying CMT2Z mutations. We observed a high number of genes with altered expression for both mutations compared to control, but in particular for the fibroblast transcriptome of the p.R252W mutation in which we noted more than 800 dysregulated genes when compared to the control fibroblast transcriptome (Fig. 5B). The clustering by functional groups for the genes with altered expression resulted in four different enrichment categories: ZNFs (zinc fingers), homeobox genes, helicases and metallothionein genes (Fig. 5C). Importantly, the transcriptomics approach showed a high percentage of repressed *ZNF*-family genes in both mutants (Fig. 5D), matching the data generated using other cellular models (21).

Neuronal features induced by overexpression of mutated MORC2 in rodent sensory neurons

Although transcriptome analysis identified evidence of an altered expression profile in patients' fibroblasts, the staining of cells with MORC2 did not show abnormal localization of the protein. Studies were therefore undertaken to evaluate the impact of MORC2 mutations in neuronal cells, which represent a relevant tissue likely to be contributing to the neurological phenotype of CMT2Z. Purified DRG sensory neurons from E15.5 rat embryos were transduced with lentivirus particles inducing expression of GFP (green fluorescent protein), WT-MORC2, or mutant (p.S87L and p.R252W) MORC2. Transduction efficiency was similar for different viral constructs (Supplementary Material, Fig. S4). Moreover, the three forms of MORC2 showed substantial overexpression of both RNA and protein in infected neurons, while MORC2 expression was undetectable in non-transduced neurons and neurons over-expressing the lentiviral GFP alone (Supplementary Material, Fig. S5). The morphology of the somas of infected neurons was unaltered by overexpression of WT or mutated forms of MORC2 (Fig. 6). The expression of endogenous Morc2 and overexpressed forms of MORC2 were predominantly detected in the nuclei of the cells. However, all forms of MORC2 were also detected in the axons (Fig. 6). Strikingly, detailed analysis of axons using SMI32 staining revealed the presence of axonal swellings in neurons expressing the p.S87L mutation (Fig. 7A). Further quantification confirmed this observation for the p.S87L mutation while the p.R252W-expressing neurons had an axonal morphology similar to the neurons expressing WT-MORC2 (Fig. 7B). As observed in sensory neurons, all forms of MORC2 also predominantly localized to the nuclei of the Schwann cells whereas the expression was undetectable in Schwann cells transfected with the plasmid containing GFP as a control (Fig. S6).

Transcriptional analysis of rat sensory neurons expressing mutated forms of MORC2

In order to perform an in-depth characterization of the consequences of the MORC2 mutated isoforms, a gene expression microarray analysis was performed. This approach was conducted on rat DRG sensory neurons expressing the WT-MORC2, the two mutated forms of MORC2 or GFP. The overexpression of the human WT-*MORC2* gene slightly altered the transcriptome profile of rat sensory neurons when compared to GFP-expressing neurons: 37 genes were upregulated and 14 showed reduced expression (Supplementary Material, Table S1). However, there was a substantial difference in the expression profiles for the two clinical variants (Fig. 8A). The analysis of the p.S87L mutation revealed that 209 genes were upregulated and 77 genes downregulated (Supplementary Material, Table S2). For the p.R252W mutation, 99 genes were found to be upregulated and 56 genes downregulated (Supplementary Material, Table S3) when compared to the GFP control.

By investigating the transcriptome-wide changes and integrating diverse types of biological data to determine pathways and networks of interest, three families of enriched genes were identified in samples expressing both mutations: *ZNF* genes, homeobox genes and neurotransmitter receptors. In addition, the kinesin family was exclusively altered in transcriptome data from the p.S87L mutant (Fig. 8B).

To investigate a possible interaction between *MORC2* and genes causing other forms of CMT, the expression of 118 rat orthologous genes associated with inherited peripheral neuropathies in humans was analyzed (Supplementary Material, Table S4). Interestingly, both mutations were associated with a strong decrease in expression of *Hspb1* ($P < 0.05$) (Fig. 8C), a gene known to cause CMT type 2F (CMT2F; MIM

606595) and distal hereditary motor neuropathy (dHMN) type IIB (dHMN2B; MIM 608634) (26). The reduced *Hspb1* expression was also confirmed by qPCR (Fig. 8D).

The *ZNF* genes represent the largest family of primate transcription factors. Thirteen *ZNF* genes were differentially expressed when comparing p.S87L and control expression profiles, with three genes significantly upregulated and ten genes downregulated ($P < 0.05$). Five dysregulated *ZNF* genes were identified when comparing p.R252W to control expression profiles, with one gene upregulated and four downregulated ($P < 0.05$) (Supplementary Material, Table S5). Altered expression levels in *ZNF* genes as repressed targets of p.R252W have previously been reported (21), and similar findings were observed using human fibroblasts (Fig. 5C).

A total of four homeobox genes were significantly dysregulated ($P < 0.01$; Fig. 8B; Supplementary Material, Table S6), which is similar to the patient fibroblast data (Fig. 5C). Both mutations showed upregulation of the *Gsc, Hoxb13* and *Hoxc10* genes. Additionally, *Hoxc6* was upregulated in p.S87L and *Hoxb8* in p.R252W (Supplementary Material, Table S6). Strikingly, changes in expression of the *Hoxb13* represent one of the highest log fold-changes observed in the transcriptome analysis.

The observed expression changes in neurotransmitter receptors and kinesins are most likely relevant for the pathophysiology of the human disease, since these families of genes may reflect pathological changes and/or compensatory mechanisms in neurons affected by CMT2Z. Within the group of neurotransmitter receptors, five genes were differentially expressed in p.S87L versus the control, with four genes upregulated and one gene significantly downregulated. Comparison of expression between p.R252W and the control identified seven upregulated and two downregulated genes (Fig. 8C). Finally, five kinesin transcripts specifically upregulated in p.S87L were detected (Fig. 8C). The latter could highlight a possible defect in anterograde axonal transport that

could contribute to the observed axonal swelling phenotype, which was induced by this mutation in sensory neuron cultures. Validation of gene expression changes in various neurotransmitter receptors was carried out by qPCR including GABA (gamma-aminobutyric acid) receptors (*Gabra1, Gabra5 and Gabrb1*) implicated in GABAergic neurotransmission in the mammalian central nervous system, and the *Grik3* encoding a glutamate receptor (Fig. 8D). Overexpression of *Kif18b*, *Kifc1* and *Kif11,* which was exclusively found with the p.S87L mutation, was confirmed by qPCR (Fig. 8D).

DISCUSSION

Including this work, 33 CMT2Z cases have been reported so far (4-13). In this study, we provide insight into the phenotypic variation of two different MORC2 mutations leading to clinical presentations ranging from axonal CMT to severe SMA.

In humans, two MORC2 transcripts have been annotated and we have shown that the transcript NM_001303256, encoding the MORC2 1,032 aa protein, is the predominant isoform expressed in neural tissues and occurs in a controlled, spatiotemporal manner. Both the Morc2 transcript and protein show peak expression at the earlier stages with a progressive decrease during aging suggesting distinct roles in developing and mature nervous systems. Interestingly, the complete loss-of-function murine model for *Morc2a* is lethal, showing growth retardation and abnormalities in neural system development (https://dmdd.org.uk/mutants/Morc2a) further supporting a developmental role for MORC2.

The *MORC2* neuropathy (CMT2Z) is the second most frequent form of axonal CMT, after CMT type 2A2 (CMT2A2; MIM 609260) which is a consequence of *MFN2* mutations (13, 27). More than half of the CMT2Z cases (17 families) are due to the

c.754C>T (p.R252W) mutation, which is *de novo* in at least 15 cases, suggesting this is a recurrent substitution because of a mutational hot spot (4-6, 8, 9, 13). It is widely established that the CpG islands are mutational hot spots due to instability of the 5-methylcytosines in DNA, and the cytosine nucleotide c.754C is located in a CpG dinucleotide. Bisulphite sequencing revealed that the c.754C remains in a predominantly methylated status favoring the mutational event, underpinning that the common p.R252W mutation is the result of spontaneous deamination of a 5-methylcytosine to yield thymine.

Both the p.R252W and the p.S87L mutations are located in the ATPase domain of MORC2. We therefore evaluated the ATPase activity for both full-length MORC2 mutations in HeLa cells and observed that only p.S87L led to a significant decrease in ATPase activity. Douse *et al*. (22) recently reported a reduced rate of ATP hydrolysis for both neuropathy-associated mutations using a construct that included the first 603 amino acids of MORC2. Together with our findings, these results demonstrate that the ATPase activity plays a role in the MORC2 function. Interestingly, both increased and decreased biochemical MORC2 activity can cause a gain-of-function phenotype probably by affecting MORC2 capacity to dimerize (22). It is therefore possible that haploinsufficiency caused by certain MORC2 mutations leads to decreased MORC2 activity manifested genetically as a dominant effect.

The observed differences in the ATPase activity for different mutations suggest that alteration of other molecular functions of MORC2 might also be contributing to the CMT2Z phenotype. Since MORC2 is known to promote the phosphorylation and activity of ACLY, an enzyme involved in the formation of acetyl-coA in the cytoplasm (18), we measured its activity in fibroblasts derived from a patient carrying p.R252W mutation as compared to a control fibroblasts. No changes in ACLY activity were

observed with the p.R252W indicating that this mutation does not impact this particular role of MORC2 in fibroblasts.

MORC2 was previously described to play a role as a transcriptional regulator. We used both the patient derived fibroblasts and rodent sensory neuron cultures to evaluate any potential morphological difference and transcriptional changes caused by an altered MORC2 function. We observed that structurally, mutant MORC2 fibroblasts did not present any morphological abnormalities compared to control cells. Interestingly, we however observed that in neurons, the p.S87L form of MORC2 led to an increase in axonal swellings, a hallmark of axonal injury. Axonal swellings have been previously described in neurodegenerative diseases, such as CMT type 2E (CMT2E; MIM 607684) caused by *NEFL* mutations (28). The axonal swelling, which represents abnormal accumulation of axonal cargos and cytoskeletal proteins, directly affects the axonal transport systems through microtubules and motor proteins (29, 30). Regarding the p.S87L mutation, a defective axonal transport could therefore underlie the pathogenesis of the neuropathy and contribute to disease severity and progression.

At the transcriptional level, our microarray data indicated enrichment of sets of genes related to *ZNF*, helicases, and homeobox genes in the human fibroblast lines carrying both investigated mutations. In addition, p.R252W fibroblasts also show altered expression in metallothionein genes. These findings were partly confirmed using rat DRG sensory neurons, since for the two used cellular models, homeobox and *ZNF* genes showed altered expression. The overexpression of homeobox genes is of interest as *Hox* genes encode conserved transcription factors regulating development and maintenance of different cellular populations (31, 32), which is compatible with the observed spatiotemporal expression pattern of *Morc2* and its suggested role in the development and maintenance of the nervous system. *ZNF* genes were previously

observed to be regulated by MORC2 (22). The *ZNF* genes are classically defined as a large family of transcription factors that can bind to DNA, RNA, lipids and proteins (33). Thus, ZNF-encoded proteins are implicated in transcriptional regulation, DNA recognition, RNA packaging, signal transduction, actin targeting, telomere maintenance, DNA repair, cell migration, and many other processes (34). In addition to the well-established involvement of the *ZNF* genes in a variety of developmental processes (35, 36), they are also implicated in diseases, including SMA (37) and Parkinson's disease (38). Collectively, these data indicate that impaired MORC2 function alters the expression of multiple transcripts involved in neuronal development.

Neurons infected with p.R252W or p.S87L showed altered expression of different neurotransmitter receptors, which are critical for basic functioning of the nervous system. In addition, expression of the *kinesin* gene group was altered in neurons expressing the p.S87L form. Within the group of neurotransmitter receptors, we observed that the genes differentially expressed included GABA receptors, a family of proteins involved in the GABAergic neurotransmission of the mammalian central nervous system (*Gabra1, Gabra5* and *Gabrb1*) and a glutamate receptor (*Grik3*), which is the predominant excitatory neurotransmitter found at synapses in the mammalian brain. The altered expression of the genes *Kif18b*, *Kifc1* and *Kif11* detected in neurons expressing the p.S87L mutation, encode kinesin proteins that are abundant in the axoplasm and are required for both fast anterograde and fast retrograde transport (29, 30). In *Drosophila* the functional disruption of kinesins leads to posterior paralysis and axonal swellings (39, 40) and deficiency in kinesins can cause neurological disorders, e.g. KIF5A dysregulation is involved in an axonal form of CMT and spastic paraplegia (41).

We also detected that the motor protein *Hspb1*, in which mutations in the human orthologue cause CMT2F, is strongly repressed in both p.R252W and p.S87L expressing neurons. It was previously shown that the expression of S135F-mutant HSPB1 in cultured mouse motor neurons led to progressive degeneration of motor neurons with disruption of the neurofilament network and aggregation of the NFL (neurofilament light) protein, encoded by the *NEFL* gene which is involved in CMT2E (42).

In conclusion, our data provide a new insight into the physiological and pathophysiological roles of MORC2 within the neural system. Both enzymatic and regulatory functions were previously linked to MORC2 (16-20). We confirmed the reported link between MORC2 and *ZNF* genes (21), which, together with observed altered expression of *homeobox* genes, indicate that MORC2 can play a role in the development of the nervous system. In the *in vitro* neuronal model used in our study, we also detected a dysregulated expression of neurotransmitter receptors, and *kinesin* genes, which encodes for proteins involved in axonal transport. Strikingly, the only altered CMT-related gene was *Hspb1*, which plays a role in the architecture of cytoskeleton. Together, the structural and transcriptional changes in neuronal cultures expressing the mutated forms of MORC2 indicate that at least part of the induced defects lead to altered axonal homeostasis. Our results therefore, contribute and support the emerging concept that alterations in axonal transport, neurofilament homeostasis and architecture of cytoskeleton are common mechanisms contributing to the CMT phenotype (43-45). Our observations warrant further exploration in particular using a human neuronal model, such as human motor neurons (MNs) derived from fibroblasts of CMT2Z patients via hiPSCs. In addition, the observed MORC2 expression in Schwann cells indicates its possible role in glia. Integration of transcriptomic, proteomic and functional

data generated from characterization of both neuronal and glial models will provide additional insight into the pathophysiology of the CMT2Z and may also help to generate suitable cellular model of the disease allowing for evaluation of relevant therapeutic strategies.

MATERIALS AND METHODS

Ethics statement

Skin biopsies from CMT2Z patients were obtained under approved by the ethics board of the corresponding hospitals where patients are supervised and written informed consents were signed.

Human first-trimester tissue was collected after elective surgical abortions with maternal oral and written informed consent. Midwives informing the patients (over 18 years old and Swedish-speaking) and responsible for the procedure of obtaining oral and written informed consent were not involved in the research study. The Regional Human Ethics Committee, Stockholm, Sweden, approved the collection. The post-conceptional age of the tissue was determined by examination of anatomical landmarks in addition to clinical ultrasound. For adult stages, the RNA was isolated from the cervical and lumbar samples of spinal cord of post-mortem subjects. Ethical approval for the use of adult human *post mortem* specimens was granted from the regional ethical review board in Stockholm, Sweden (Regionala Etikprövnings nämnden, Stockholm, EPN). All adult human spinal cord samples were obtained from the Netherlands Brain Bank (NBB, http://www.brainbank.nl) and the National Disease Research Interchange (NDRI, http://www.ndriresource.org) with the written informed consent from the donors or next of kin.

Rat and mice were sacrificed by exposure to CO_2. All animal work was performed in accordance with the Swedish regulations and approved by the regional ethics review committee Stockholm, Stockholms norra djurförsöksetiska nämnd (N79/15).

Expression of MORC2 isoforms in human nervous tissues

Total RNA was isolated from DRGs dissected from human first trimester tissues collected at 7.5, 8-8.5 and 9 weeks post-conception.

Total RNA was extracted using Direct-zol™ RNA MiniPrep Plus (Zymo Research, Irvine, CA, USA) and the reverse transcribed template was prepared from 0.5 µg of total RNA using PrimeScript Reverse Transcriptase (Takara, Noji-higashi, Japan). Expression of MORC2 isoforms was measured after PCR amplification with the primer pairs hMORC2_1, hMORC2_2, and hMORC2_3 (Supplementary Material, Table S7). Normalization and amplification efficiency was confirmed using human actin primers.

Spatiotemporal analysis of Morc2 expression in mice peripheral nervous system

Total RNA from brain, spinal cord, DRG and sciatic nerve at different development stages was isolated using RNeasy Plus Mini Kit (Qiagen, Hilden, Germany). Direct-zol™ RNA MiniPrep Plus (Zymo Research, Irvine, CA, USA) was used to extract RNA from cultured neurons and Schwann cells. The reverse transcribed template was prepared from 1 µg of total RNA using the QuantiTect Reverse Transcription Kit (Qiagen, Hilden, Germany). Morc2 was amplified by RT-PCR using the primer pairs: mMorc2a-1 and mMorc2a-2 (Supplementary Material, Table S7). The expression was normalized using the endogenous mouse gene *Ubiquitin2l3* (primers Ubi2l3).

Brain and sciatic nerve protein extracts were obtained from mice at selected time points using a polytron homogenizer and RIPA lysis buffer (50mM Tris-HCl pH 7.4, 5mM DL-Dithiothreitol - DTT, 150mM NaCl, 1% NP-40, 0.5% deoxycolate). A rabbit polyclonal Morc2 antibody (Santa Cruz Biotechnology, Dallas, TX, USA) was used to perform immunoblotting studies.

Bisulphite Sequencing

Genomic DNA (2 µg) was treated with sodium bisulphite using the EpiTect Bisulphite Kit (Qiagen, Hilden, Germany). Nested PCR was used to amplify a 278 bp fragment encompassing the MORC2 R252 residue. The first round of PCR was performed in a total volume of 25 µl using 2 µg of purified bi-sulphite treated DNA, 0.4 µM of each primer compatible with bisulphite-converted sequence and MyTaq HS Red Mix (Bioline, London, UK). Nested PCR was performed using the same primers and reagent concentration with template (1.5 µl) from the first round of PCR. The PCR amplicon was gel purified using the ISOLATE II PCR and Gel Kit and cloned into the pCR4-TOPO TA vector (Thermo Fisher Scientific, Waltham, MA, USA). Nineteen clones were sequenced using BigDye Terminator v3.1 Cycle Sequencing protocols at the ACRF (Australian Cancer Research Foundation) facility (Garvan Institute of Medical Research, Darlinghurst, Australia).

MORC2 immunofluorescence in human fibroblast derived from CMT2Z patients

Fibroblast cell lines grown in DMEM (Dulbecco's Modified Eagle's Medium) without glucose (DMEM, 10% heat-inactivated fetal bovine serum - FBS, 1% L-glutamine, 1% Penicillin/Streptomycin - P/S and 1% Sodium Pyruvate), were fixed in 4% paraformaldehyde, permeabilized with Triton 0.25% in PBS and incubated in blocking

buffer (5% Horse Serum in phosphate-buffered saline - PBS) for 1h at RT. The primary antibody anti-MORC2 (Santa Cruz Biotechnology, Dallas, TX, USA) was incubated in blocking buffer overnight (o/n) at 4°C. The next day, samples were incubated with the appropriate secondary antibody (Alexa-488, Thermo Fisher Scientific, Waltham, MA, USA) in blocking buffer during 1h at RT and mounted with Vectashied including DAPI (Vector laboratories, Burlingame, CA, USA). Slides were examined with LSM880 confocal microscope (Zeiss, Oberkochen, Germany).

Generation of lentiviral vectors

For the overexpression experiment, lentiviral particles were produced by co-transfecting 293T cells with the lentiviral vector pSlik-Hygro (Addgene, Cambridge, MA, USA) containing GFP as a control, human WT-MORC2, MORC2 p.R252W, MORC2 p.S87L (under an inducible Doxycycline promoter) and the co-vectors PLP1, PLP2 and PLP/VSVG (Invitrogen, Carlsbad, CA, USA). Cells were incubated at 37°C and 5% CO_2 and 12 h after transduction the medium (DMEM) supplemented with 10% (v/v) FBS and 1% (v/v) P/S was replaced. The conditioned medium was harvested after 48 h. The viruses were concentrated by 4 h centrifugation at 24,000 rcf at 4°C, aliquoted and stored at -80°C.

Generation of continuous cell lines overexpressing MORC2 and ATPase assay

HeLa cells grown in DMEM plus (DMEM, 10% (v/v) heat-inactivated FBS, 5g/L D-glucose, 1% (v/v) L-glutamine and 1% (v/v) P/S), were exposed to lentiviruses containing GFP, WT-MORC2 or MORC2 mutants (p.S87L and p.R252W) for 12 h and were selected with 4 cycles of DMEM plus supplemented with 200 µg/mL of Hygromycin, changing the medium every 2 days post-infection. The transgene

511 expression was induced by exposure to DMEM plus with 2 µg/mL of Doxycycline for 4
512 days. The nuclear extracts were prepared using an extraction method by high salt
513 concentration as described previously (20) and kept on ice while the protein was
514 quantified with BCA kit (Thermo Fisher Scientific, Waltham, MA, USA). For the
515 ATPase assay, 50 µg of nuclear protein was used in the High Throughput Colorimetric
516 ATPase Assays (Innova Bioscience, San Diego, CA, USA). The data were presented as
517 the average ± the standard deviation for three independent assays and the results were
518 normalized with the uninfected control set to 1. Statistical significance was determined
519 by two-tailed Student's t test and considered statistically significant when P was <0.05.
520 In order to confirm an equal MORC2 overexpression for all the samples, 30 µg of
521 protein was loaded on a 10% (v/v) polyacrylamide gel under reducing conditions.
522 Membranes were blocked by incubation with 5% w/v milk powder in TBST (25 mm
523 Tris-HCl, 150 mm NaCl, 0.05% v/v Tween 20, pH 7.4) for 1 h at RT. For
524 immunodetection, the polyvinylidene difluoride (PVDF) membranes were incubated o/n
525 with anti-MORC2 1:250 (v/v) (Santa Cruz Biotechnology, Dallas, TX, USA) and anti-
526 Actin 1:2000 (v/v) (Sigma-Aldrich, St. Louis, MI, USA) diluted in 3% w/v BSA
527 (bovine serum albumin) in TBST. The day after, the appropriate secondary HRP
528 (horseradish peroxidase)-conjugated antibodies were incubated for 1 h at RT using a
529 dilution of 1:10000 (v/v), followed by exposure to a film (Fujifilm, Tilburg, The
530 Netherlands).
531
532 **ACLY activity enzyme assay**
533 ACLY enzyme activity was indirectly assayed using the commercial MDH Colorimetric
534 Kit (Biovision, Milpitas, CA, USA) according to the manufacturer's instructions.
535 Absorbance readings at 450 nm were taken at 1 min interval for 20 min at 37 °C using

536 an EnSpire Multimode Plate Reader (Perkin Elmer, Waltham, MA, USA) to monitor
537 NADH production. Cell extracts from the patient (p.R252W) and control fibroblasts
538 were used for the assay. The assay was performed for three independent experiments
539 and the mean ± SEM (standard error of the mean) MDH activity was calculated.
540
541 **Preparation of rat sensory neuron cultures**
542 DRGs were dissected from rat Sprague-Dawley embryos at embryonic day 14.5
543 (E14.5). Dissected DRGs were triturated in 0.25% (v/v trypsin containing 0.25% (v/v)
544 EDTA for 1 h at 37°C, harvested by soft centrifugation (100 rcf for 15 min) and
545 resuspended in C-medium (DMEM with 10% (v/v) Fetal Calf Serum - FCS, 1% (v/v)
546 P/S, 200 mM L-glutamine, 50 µg/mL 2.5S Nerve Growth Factor - NGF). Cells were
547 plated at a concentration of 1.5 DRG per 12 mm glass covers coated by growth factor
548 reduced Matrigel (Clontech, Fremont, CA, USA) or Poly-L-Lysine (Sigma-Aldrich, St.
549 Louis, MI, USA) o/n at 37°C and 5% CO_2. The day after, the medium was replaced by
550 Neurobasal (NB)-supplemented medium (NB medium with 2 g/L D-glucose, 1X B27
551 supplement, 1% P/S (v/v), 200 mM L-glutamine and 50 µg/mL 2.5S NGF) and cultured
552 for one week replacing the medium every 2 days. To archive pure neuron cultures,
553 dissociated DRG cultures were cycled for three weeks between NB-supplemented
554 medium and NB-supplemented medium with 10 µM Fluorodeoxyuridine (Sigma-
555 Aldrich, St. Louis, MI, USA).
556
557 **Overexpression of mutated forms of MORC2 in rat sensory neurons**
558 Neuronal cultures were infected with lentivirus containing GFP, WT-MORC2, MORC2
559 p.S87L and MORC2 p.R252W in NB-supplemented medium for 12 h and were selected

using 200 µg/mL of Hygromycin for one week. The overexpression of the transgene was induced with 2 µg/mL of Doxycycline for 4 days.

Immunofluorescence assays, RNA and protein extraction of neuronal cultures

For the immunofluorescence assays, dissociated DRG neurons were fixed in 4% (v/v) paraformaldehyde and incubated in blocking buffer (5% (v/v) Normal Goat Serum - NGS, 1% BSA (v/v) and 0.3% (v/v) Triton X-100 in PBS) for 1 h at RT and washed in PBS. The primary antibodies anti-MORC2 (Santa Cruz Biotechnology, Dallas, TX, USA) and anti-SMI32 (Millipore, Burlington, MA, USA) were incubated in blocking buffer + PBS in a dilution 1:1 o/n at 4°C. The next day, samples were incubated with the appropriate secondary antibodies conjugated with fluorophores (Alexa-488 or Alexa-594, Thermo Fisher Scientific, Waltham, MA, USA) in PBS for 1 h at RT, stained with DAPI, dried and mounted with Vectashied (Vector laboratories, Burlingame, CA, USA). Slides were examined with LSM880 confocal microscope (Zeiss, Oberkochen, Germany). To confirm the overexpression, total RNA was extracted using Direct-zol™ RNA MiniPrep Plus (Zymo Research, Irvine, CA, USA) and 0.150 µg was employed to prepare reverse transcribed template using "PrimeScript Reverse Transcriptase" (Takara, Noji-higashi, Japan). *MORC2* expression was examined through RT-PCR with the primer pair hMORC2_4 (S7 Table). Equal cDNA loading was established using primers against actin. For western-blot analysis, the neurons were kept on ice with ice-cold lysis buffer (25 mm Tris-HCl pH 7.5, 95 mm NaCl, 10 mm EDTA, 2% (v/v) sodium dodecyl sulfate - SDS, 1 mm NaF and 1 mm $NaVO_4$ in PBS) for 30 min and were homogenized with tissue-lyser. Proteins lysates were obtained through centrifugation at 4°C and 16,000 rcf for 10 min with protein concentration determined using the BCA kit (Thermo Fisher Scientific, Waltham, MA,

585 USA). Finally, the tubes were boiled during 5 min and stored at -80°C. For SDS-PAGE
586 (polyacrylamide gel electrophoresis), 30 µg of proteins from each sample were
587 separated on a 10% (v/v) polyacrylamide gel under reducing conditions. After the
588 blocking with 5% w/v milk powder in TBST during 1h at RT, the membranes were
589 incubated o/n with anti-MORC2 (Santa Cruz Biotechnology, Dallas, TX, USA) and
590 anti-Actin (Sigma-Aldrich, St. Louis, MI, USA) diluted in 3% w/v BSA in TBST and
591 the next day, the appropriate secondary HRP-conjugated antibodies were incubated for
592 1h at RT, followed by developing on a film (Fujifilm, Tilburg, The Netherlands).
593
594 **Generation of primary rat Schwann cells transiently overexpressing MORC2**
595 Primary rat Schwann cells have been cultured as previously described (46). Briefly,
596 sciatic nerves of P3 Sprague-Dawley rats were collected and dissociated in 1 mL
597 DMEM plus 300 µl of 10 mg/mL collagenase (Worthington, Columbus, OH, USA).
598 The tissue was subsequently incubated with 0.25% trypsin (Gibco, Thermo Fisher
599 Scientific, Waltham, MA, USA) and plated in DMEM with 10% FCS (Gibco, Thermo
600 Fisher Scientific, Waltham, MA, USA). The purity of culture was achieved by depletion
601 of fibroblast using anti–Thy 1.1 antibody (Millipore, Burlington, MA, USA) and rabbit
602 complement (Sigma-Aldrich, St. Louis, MI, USA). Pure rat Schwann cells were
603 expanded in DMEM supplemented with 10% FCS, 4 mM forskolin (Sigma-Aldrich, St.
604 Louis, MI, USA) and 10 ng/mL of human recombinant NRG1-beta 1 (R&D System,
605 Minneapolis, MN, USA).
606 The transient overexpression of the MORC2 isoforms was achieved by
607 transfecting the Schwann cells with pcDNA3,1 containing GFP as a control, human
608 WT-MORC2, MORC2 p.R252W and MORC2 p.S87L (under CMV promoter). 48

hours after the transfection the cells were fixed with 4%PFA in PBS and the immunofluorescence has been performed as described for the DRG neurons.

Analysis of axonal swellings in infected rat sensory neurons

The average number of axonal swellings was calculated based on 15 pictures from each sample immunostained with SMI32 (Millipore, Burlington, MA, USA) per infection. All the data were reported as the sample mean ± SEM for three independent lentiviral infections of the neuronal cultures and the results were normalized with the control sample. Pairwise comparisons between means of different groups were performed using a Student t-test (two tailed, unpaired) and considered statistically significant when $P < 0.05$.

Transcriptome analysis in human fibroblast and rat sensory neurons

The quality and quantity of RNA was evaluated by spectrometry (NanoDrop ND1000, NanoDrop Technologies, Wilminton, Delaware USA) and by RNA 6000 Nano Bioanalyzer (Agilent Technologies, Palo Alto, CA, USA) assays (Supplementary Material, Table S8). Two hundred ng of total RNA were used to produce Cyanine 3-CTP-labeled cRNA using the One-Color Low Input Quick Amp Labeling Kit (Agilent p/n 5190-2305) according to the manufacturer's instructions. Following One-Color Microarray-Based Gene Expression Analysis protocol Version 6.7 (Agilent p/n G4140-90040), 600 ng of labeled cRNA was hybridized with the SurePrint G3 Rat Gene Expression v2 8x60K Microarray (Agilent p/n G4858A-074036) containing 30,584 Entrez Genes (unique) and SurePrint G3 Human Gene Expression v3 8x60K Microarray (Agilent p/n G4858A-072363) containing 26,083 Entrez Genes (unique) + 30,606 lncRNAs (unique). Arrays were scanned in an Agilent Microarray Scanner (Agilent

G2565C) according to the manufacturer's protocol and data extracted using Agilent Feature Extraction Software 11.5.1.1 following the Agilent protocol GE1_1105_Oct12, grid templates 072363_D_F_20150612 and 074036_D_F_20150914 and the QC Metric Set GE1_QCMT_Oct12. Agilent Processed Signal (Agilent Feature Extraction Software) was standardized using quantile normalization (47). Differential gene expression was carried out using the *limma* (48) package from Bioconductor. Multiple testing adjustments of *P* were performed according to the False Discovery Rate method (49, 50). Gene enrichment analysis was carried out with DAVID Bioinformatics Resources, version 6.8 (51).

ACKNOWLEDGEMENTS

We thank Hasna Baloui, Enric Domènech-Estévez and Jean-Jacques Médard at the KI, and Ana Sánchez-Monteagudo, Dolores Martínez-Rubio and Virginia Rejas at the CIPF, for their technical assistance. First trimester human tissue was acquired through the KI Stem Cell and Tissue Bank, financed and supported by CIMED. Adult human tissue was acquired through Netherlands Brain Bank (NBB, www.brainbank.nl) and the National Disease Research Interchange (NDRI, www.ndriresource.org). This work was supported by the Instituto de Salud Carlos III (ISCIII) - Subdirección General de Evaluación y Fomento de la Investigación within the framework of the National R+D+I Plan [grant number PI15/00187 to C.E. and PI16/00403 to T.S.], co-funded with FEDER funds; by the Ramón Areces Foundation [grant number CIVP17A2810 to C.E]; by the Generalitat Valenciana [grant number PROMETEO/2018/135 to C.E. and T.S.]; by the AFM-Téléthon [grant number 21500 to C.E. and R.C.]; by National Health and Medical Research Council of Australia Grant [grant number APP1046680 to M.K.], by grant from the Czech Health Research Council [grant number AZV16-30206A to P.L.];

659 by the Swedish StratNeuro program grant and by the Swedish Research Council [grant
660 number 2015-02394 to R.C.]. C.E. had a “Miguel Servet” contract funded by the ISCIII
661 and the Centro de Investigación Príncipe Felipe (CIPF) [grant number CPII14/00002].
662 P.S. is the recipient of a FPU-PhD fellowship funded by the Spanish Ministry of
663 Education, Culture and Sport [FPU15/00964]. The funders had no role in study design,
664 data collection and analysis, decision to publish, or preparation of the manuscript.
665
666
667 **Conflict of interest statement**
668 The authors declare that they have no conflicts of interest.
669
670

671 **REFERENCES**

672 1 Dyck, P., Lambert , EH. (1968) Lower motor and primary sensory neuron
673 diseases with peroneal muscular atrophy. I. Neurologic, genetic, and electrophysiologic
674 findings in hereditary polyneuropathies. *Arch. Neurol.*, **18**, 603-618.

675 2 Szigeti, K. and Lupski, J.R. (2009) Charcot-Marie-Tooth disease. *Eur. J. Hum.*
676 *Genet.*, **17**, 703-710.

677 3 Pareyson, D. and Marchesi, C. (2009) Diagnosis, natural history, and
678 management of Charcot-Marie-Tooth disease. *Lancet Neurol.*, **8**, 654-667.

679 4 Sevilla, T., Lupo, V., Martinez-Rubio, D., Sancho, P., Sivera, R., Chumillas,
680 M.J., Garcia-Romero, M., Pascual-Pascual, S.I., Muelas, N., Dopazo, J. *et al.* (2016)
681 Mutations in the MORC2 gene cause axonal Charcot-Marie-Tooth disease. *Brain*, **139**,
682 62-72.

683 5 Albulym, O.M., Kennerson, M.L., Harms, M.B., Drew, A.P., Siddell, A.H.,
684 Auer-Grumbach, M., Pestronk, A., Connolly, A., Baloh, R.H., Zuchner, S. *et al.* (2016)
685 MORC2 mutations cause axonal Charcot-Marie-Tooth disease with pyramidal signs.
686 *Ann. Neurol.*, **79**, 419-427.

687 6 Lassuthova, P., Safka Brozkova, D., Krutova, M., Mazanec, R., Zuchner, S.,
688 Gonzalez, M.A. and Seeman, P. (2016) Severe axonal Charcot-Marie-Tooth disease
689 with proximal weakness caused by de novo mutation in the MORC2 gene. *Brain*, **139**,
690 e26.

691 7 Zhao, X., Li, X., Hu, Z., Liu, L., Xie, Y., Tian, T., Man, J., Wang, J., Zi, X., Xia,
692 K. *et al.* (2016) MORC2 mutations in a cohort of Chinese patients with Charcot-Marie-
693 Tooth disease type 2. *Brain*, **139**, e56.

8 Hyun, Y.S., Hong, Y.B., Choi, B.O. and Chung, K.W. (2016) Clinico-genetics in Korean Charcot-Marie-Tooth disease type 2Z with MORC2 mutations. *Brain*, **139**, e40.

9 Bansagi, B., Griffin, H., Whittaker, R.G., Antoniadi, T., Evangelista, T., Miller, J., Greenslade, M., Forester, N., Duff, J., Bradshaw, A. *et al.* (2017) Genetic heterogeneity of motor neuropathies. *Neurology*, **88**, 1226-1234.

10 Schottmann, G., Wagner, C., Seifert, F., Stenzel, W. and Schuelke, M. (2016) MORC2 mutation causes severe spinal muscular atrophy-phenotype, cerebellar atrophy, and diaphragmatic paralysis. *Brain*, **139**, e70.

11 Semplicini, C., Ollagnon-Roman, E., Leonard-Louis, S., Piguet-Lacroix, G., Silvestre, M., Latour, P. and Stojkovic, T. (2017) High intra-familiar clinical variability in MORC2 mutated CMT2 patients. *Brain*, **140**, e21.

12 Zanni, G., Nardella, M., Barresi, S., Bellacchio, E., Niceta, M., Ciolfi, A., Pro, S., D'Arrigo, S., Tartaglia, M. and Bertini, E. (2017) De novo p.T362R mutation in MORC2 causes early onset cerebellar ataxia, axonal polyneuropathy and nocturnal hypoventilation. *Brain*, **140**, e34.

13 Ando, M., Okamoto, Y., Yoshimura, A., Yuan, J.H., Hiramatsu, Y., Higuchi, Y., Hashiguchi, A., Mitsui, J., Ishiura, H., Fukumura, S. *et al.* (2017) Clinical and mutational spectrum of Charcot-Marie-Tooth disease type 2Z caused by MORC2 variants in Japan. *Eur. J. Neurol.*, **24**, 1274-1282.

14 Inoue, N., Hess, K.D., Moreadith, R.W., Richardson, L.L., Handel, M.A., Watson, M.L. and Zinn, A.R. (1999) New gene family defined by MORC, a nuclear protein required for mouse spermatogenesis. *Hum. Mol. Genet.*, **8**, 1201-1207.

15 Iyer, L.M., Abhiman, S. and Aravind, L. (2008) MutL homologs in restriction-modification systems and the origin of eukaryotic MORC ATPases. *Biol. Direct.*, **3**, 8.

16 Shao, Y., Li, Y., Zhang, J., Liu, D., Liu, F., Zhao, Y., Shen, T. and Li, F. (2010) Involvement of histone deacetylation in MORC2-mediated down-regulation of carbonic anhydrase IX. *Nucleic Acids Res.*, **38**, 2813-2824.

17 Liao, X.H., Zhang, Y., Dong, W.J., Shao, Z.M. and Li, D.Q. (2017) Chromatin remodeling protein MORC2 promotes breast cancer invasion and metastasis through a PRD domain-mediated interaction with CTNND1. *Oncotarget*, **8**, 97941-97954.

18 Sanchez-Solana, B., Li, D.Q. and Kumar, R. (2014) Cytosolic functions of MORC2 in lipogenesis and adipogenesis. *Biochim. Biophys. Acta*, **1843**, 316-326.

19 Tong, Y., Li, Y., Gu, H., Wang, C., Liu, F., Shao, Y., Li, J., Cao, L. and Li, F. (2015) Microchidia protein 2, MORC2, downregulates the cytoskeleton adapter protein, ArgBP2, via histone methylation in gastric cancer cells. *Biochem. Biophys. Res. Commun.*, **467**, 821-827.

20 Li, D.Q., Nair, S.S., Ohshiro, K., Kumar, A., Nair, V.S., Pakala, S.B., Reddy, S.D., Gajula, R.P., Eswaran, J., Aravind, L. *et al.* (2012) MORC2 signaling integrates phosphorylation-dependent, ATPase-coupled chromatin remodeling during the DNA damage response. *Cell. Rep.*, **2**, 1657-1669.

21 Tchasovnikarova, I.A., Timms, R.T., Douse, C.H., Roberts, R.C., Dougan, G., Kingston, R.E., Modis, Y. and Lehner, P.J. (2017) Hyperactivation of HUSH complex function by Charcot-Marie-Tooth disease mutation in MORC2. *Nat. Genet.*, **49**, 1035-1044.

22 Douse, C.H., Bloor, S., Liu, Y., Shamin, M., Tchasovnikarova, I.A., Timms, R.T., Lehner, P.J. and Modis, Y. (2018) Neuropathic MORC2 mutations perturb GHKL ATPase dimerization dynamics and epigenetic silencing by multiple structural mechanisms. *Nat. Commun.*, **9**, 651.

743 23 Frasquet, M., Mas, F., Vázquez-Costa, J.F., Espinós, C., Lupo, V. and Sevilla, T.
744 (2018), In *15th International Congress on Neuromuscular Diseases*, Vienna, pp. S258.
745 24 Szutowicz, A., Bielarczyk, H., Jankowska-Kulawy, A., Pawelczyk, T. and
746 Ronowska, A. (2013) Acetyl-CoA the key factor for survival or death of cholinergic
747 neurons in course of neurodegenerative diseases. *Neurochem. Res.*, **38**, 1523-1542.
748 25 Lopez-Ibarra, Z., Modrego, J., Valero-Munoz, M., Rodriguez-Sierra, P.,
749 Zamorano-Leon, J.J., Gonzalez-Cantalapiedra, A., de Las Heras, N., Ballesteros, S.,
750 Lahera, V. and Lopez-Farre, A.J. (2015) Metabolic differences between white and
751 brown fat from fasting rabbits at physiological temperature. *J. Mol. Endocrinol.*, **54**,
752 105-113.
753 26 Evgrafov, O.V., Mersiyanova, I., Irobi, J., Van Den Bosch, L., Dierick, I.,
754 Leung, C.L., Schagina, O., Verpoorten, N., Van Impe, K., Fedotov, V. *et al.* (2004)
755 Mutant small heat-shock protein 27 causes axonal Charcot-Marie-Tooth disease and
756 distal hereditary motor neuropathy. *Nat. Genet.*, **36**, 602-606.
757 27 Pareyson, D., Saveri, P. and Pisciotta, C. (2017) New developments in Charcot-
758 Marie-Tooth neuropathy and related diseases. *Curr. Opin. Neurol.*, **30**, 471-480.
759 28 Fabrizi, G.M., Cavallaro, T., Angiari, C., Cabrini, I., Taioli, F., Malerba, G.,
760 Bertolasi, L. and Rizzuto, N. (2007) Charcot-Marie-Tooth disease type 2E, a disorder of
761 the cytoskeleton. *Brain*, **130**, 394-403.
762 29 Martin, M., Iyadurai, S.J., Gassman, A., Gindhart, J.G., Jr., Hays, T.S. and
763 Saxton, W.M. (1999) Cytoplasmic dynein, the dynactin complex, and kinesin are
764 interdependent and essential for fast axonal transport. *Mol. Biol. Cell.*, **10**, 3717-3728.
765 30 Goldstein, L.S. (2001) Kinesin molecular motors: transport pathways, receptors,
766 and human disease. *Proc. Natl. Acad. Sci. U. S. A.*, **98**, 6999-7003.

31 Nichterwitz, S., Chen, G., Aguila Benitez, J., Yilmaz, M., Storvall, H., Cao, M., Sandberg, R., Deng, Q. and Hedlund, E. (2016) Laser capture microscopy coupled with Smart-seq2 for precise spatial transcriptomic profiling. *Nat. Commun.*, **7**, 12139.

32 Nolte, C.A., Tara, B. and Krumlauf, R. (2015) John and Wiley & Sons, L. (eds.), In *eLS: Essential for Life Science*.

33 Matthews, J.M. and Sunde, M. (2002) Zinc fingers--folds for many occasions. *IUBMB Life*, **54**, 351-355.

34 Cassandri, M., Smirnov, A., Novelli, F., Pitolli, C., Agostini, M., Malewicz, M., Melino, G. and Raschella, G. (2017) Zinc-finger proteins in health and disease. *Cell. Death. Discov.*, **3**, 17071.

35 Merzdorf, C.S. (2007) Emerging roles for zic genes in early development. *Dev. Dyn.*, **236**, 922-940.

36 Aruga, J. (2004) The role of Zic genes in neural development. *Mol. Cell. Neurosci.*, **26**, 205-221.

37 Ahmad, S., Wang, Y., Shaik, G.M., Burghes, A.H. and Gangwani, L. (2012) The zinc finger protein ZPR1 is a potential modifier of spinal muscular atrophy. *Hum. Mol. Genet.*, **21**, 2745-2758.

38 Shin, J.H., Ko, H.S., Kang, H., Lee, Y., Lee, Y.I., Pletinkova, O., Troconso, J.C., Dawson, V.L. and Dawson, T.M. (2011) PARIS (ZNF746) repression of PGC-1alpha contributes to neurodegeneration in Parkinson's disease. *Cell*, **144**, 689-702.

39 Gindhart, J.G., Jr., Desai, C.J., Beushausen, S., Zinn, K. and Goldstein, L.S. (1998) Kinesin light chains are essential for axonal transport in Drosophila. *J. Cell. Biol.*, **141**, 443-454.

790 40 Hurd, D.D. and Saxton, W.M. (1996) Kinesin mutations cause motor neuron
791 disease phenotypes by disrupting fast axonal transport in Drosophila. *Genetics*, **144**,
792 1075-1085.
793 41 Crimella, C., Baschirotto, C., Arnoldi, A., Tonelli, A., Tenderini, E., Airoldi, G.,
794 Martinuzzi, A., Trabacca, A., Losito, L., Scarlato, M. *et al.* (2012) Mutations in the
795 motor and stalk domains of KIF5A in spastic paraplegia type 10 and in axonal Charcot-
796 Marie-Tooth type 2. *Clin. Genet.*, **82**, 157-164.
797 42 Zhai, J., Lin, H., Julien, J.P. and Schlaepfer, W.W. (2007) Disruption of
798 neurofilament network with aggregation of light neurofilament protein: a common
799 pathway leading to motor neuron degeneration due to Charcot-Marie-Tooth disease-
800 linked mutations in NFL and HSPB1. *Hum. Mol. Genet.*, **16**, 3103-3116.
801 43 Azzedine, H., Senderek, J., Rivolta, C. and Chrast, R. (2012) Molecular genetics
802 of charcot-marie-tooth disease: from genes to genomes. *Mol. Syndromol.*, **3**, 204-214.
803 44 Bucci, C., Bakke, O. and Progida, C. (2012) Charcot-Marie-Tooth disease and
804 intracellular traffic. *Prog. Neurobiol.*, **99**, 191-225.
805 45 Gentil, B.J. and Cooper, L. (2012) Molecular basis of axonal dysfunction and
806 traffic impairments in CMT. *Brain Res. Bull.*, **88**, 444-453.
807 46 Bartesaghi, L., Arnaud Gouttenoire, E., Prunotto, A., Medard, J.J., Bergmann, S.
808 and Chrast, R. (2015) Sox4 participates in the modulation of Schwann cell myelination.
809 *Eur. J. Neurosci.*, **42**, 1788-1796.
810 47 Bolstad, B.M., Irizarry, R.A., Astrand, M. and Speed, T.P. (2003) A comparison
811 of normalization methods for high density oligonucleotide array data based on variance
812 and bias. *Bioinformatics*, **19**, 185-193.

48 Smyth, G.K. (2004) Linear models and empirical bayes methods for assessing differential expression in microarray experiments. *Stat. Appl. Genet. Mol. Biol.*, **3**, Article3.

49 Benjamini, Y. and Hochberg, Y. (1995) Controlling the false discovery rate: a practical and powerful approach to multiple testing. *J. R. Statist. Soc. B*, **57**, 289-300.

50 Benjamini, Y., Drai, D., Elmer, G., Kafkafi, N. and Golani, I. (2001) Controlling the false discovery rate in behavior genetics research. *Behav. Brain. Res.*, **125**, 279-284.

51 Huang da, W., Sherman, B.T. and Lempicki, R.A. (2009) Systematic and integrative analysis of large gene lists using DAVID bioinformatics resources. *Nat. Protoc.*, **4**, 44-57.

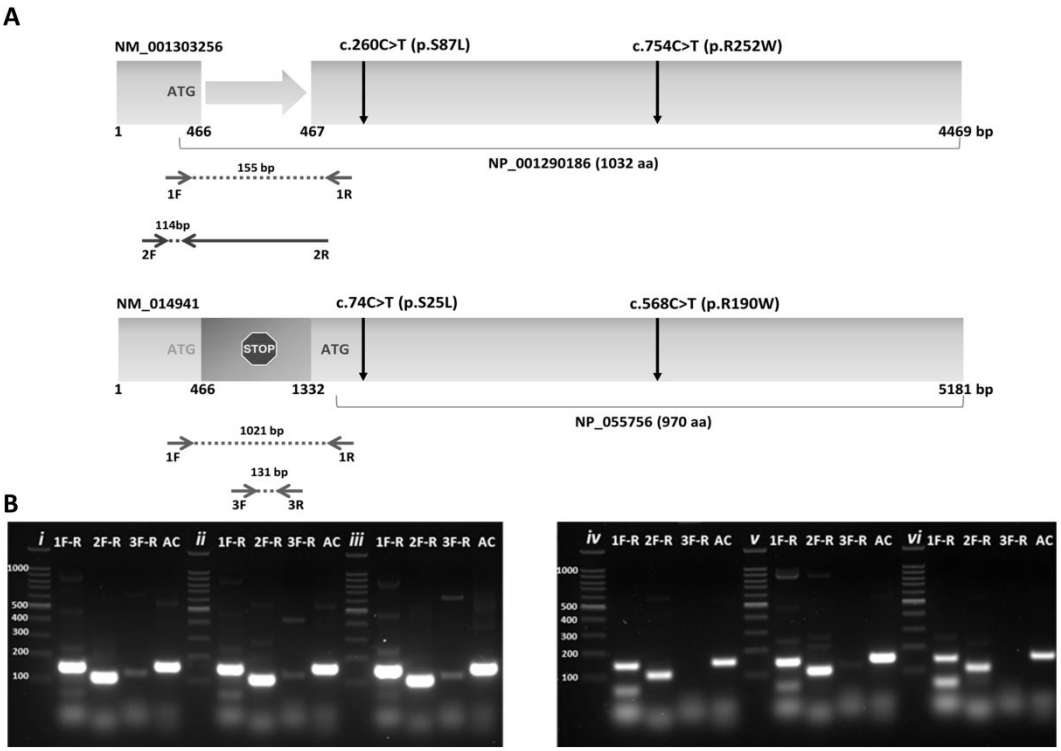

826

827 **Figure 1.** Characterization of the expression of MORC2 isoforms in nervous system.
828 **(A)** Schematic representation of the two MORC2 transcripts, showing the position of
829 designed primers and amplicon sizes. Primer pair 1F-1R was designed to amplify the
830 two isoforms with different amplicon sizes (155 bp for NM_001303256 and 1021 bp for
831 NM_014941); primer pair 2F-2R was designed to amplify only the NM_001303256
832 isoform with an amplicon size of 114 bp. Primer pair 3F-3R was designed internally to
833 the absent fragment in NM_001303256, to specifically amplify the NM_014941 with an
834 amplicon of size of 131 bp. **(B)** RT-PCR characterization of MORC2 expression using
835 the aforementioned primers and cDNA template prepared from DRGs isolated from
836 aborted human embryos of different ages (i: 7.5 weeks, ii: 8-8.5 weeks, iii: 9 weeks) and
837 neurons isolated from adult spinal cord (iv, v: cervical region, vi: lumbar region).
838 Human *actin* was used as a control (AC).

839

840

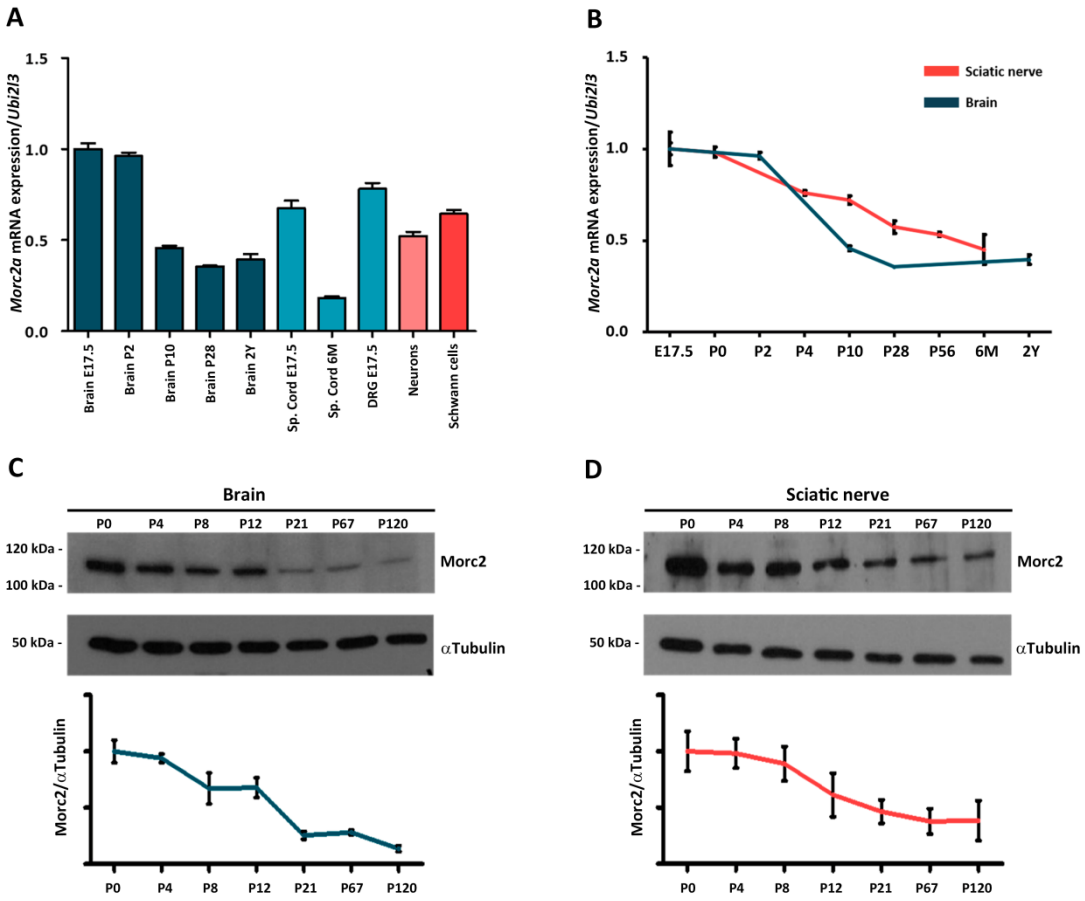

Figure 2. Characterization of the Morc2 expression profiles during neuronal development. **(A, B)** Quantitative-PCR of the *Morc2a* expression in several mice nervous tissues and cells. The relative expression levels of *Morc2a* at the different time points was normalized using Ubiquitin (*Ubi2l3*) with the brain expression at E17.5 being set to 1. **(C, D)** Western-blot based quantification of Morc2 protein in mice brain **(C)** and sciatic nerve **(D)** samples isolated at selected time points. □□Tubulin was used to normalize the amount of loaded protein. The relative protein levels for each time point were obtained using the brain at P0 set as +1. E=Embryonic stage, P=Post-natal day, M=Months, Y=Years.

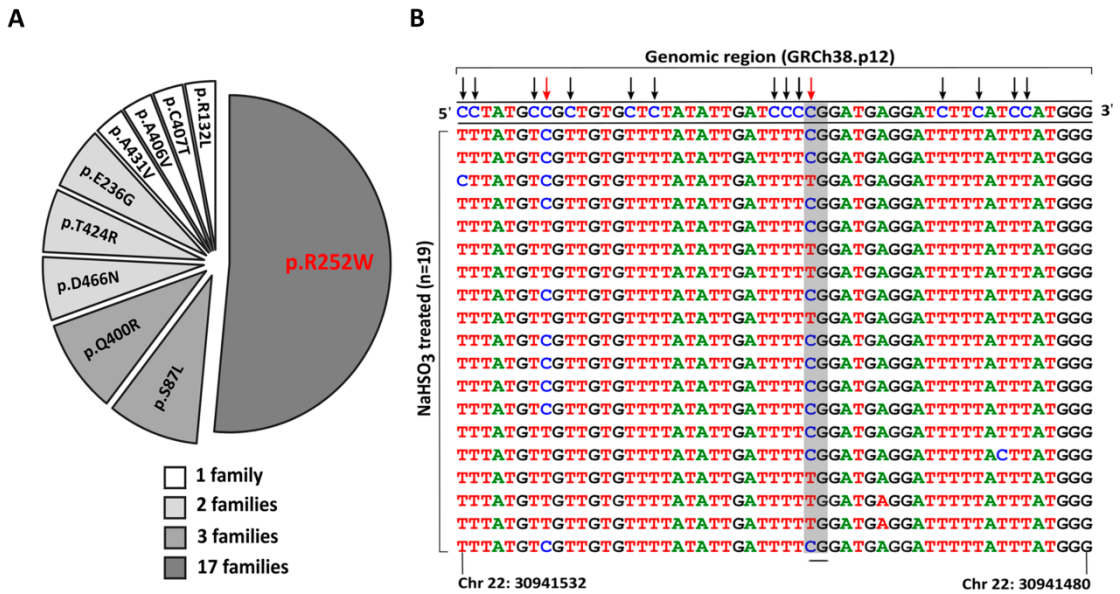

Figure 3. Genetics of CMT2Z. **(A)** Distribution of *MORC2* mutations identified in CMT2Z patients, using protein nomenclature (NP_001290186). **(B)** Characterization of the methylation status of CpG dinucleotides in exon 10 of the *MORC2* gene (NM_001303256) using bisulphite sequencing analysis. Sequence from n=19 clones of bisulphite-treated DNA containing the c.754C nucleotide are aligned to the genomic consensus sequence (underlined sequence on the top of the panel). Converted (black arrows) and non-converted (red arrows) cytosines are shown. Non-CpG cytosines are converted to thymidine and most of the CpG cytosines for each clone remain unchanged, which indicates that nucleotide position c.754 can have 5-methylcytosine nucleotides. The CpG dinucleotide containing c.754C is remarked in grey.

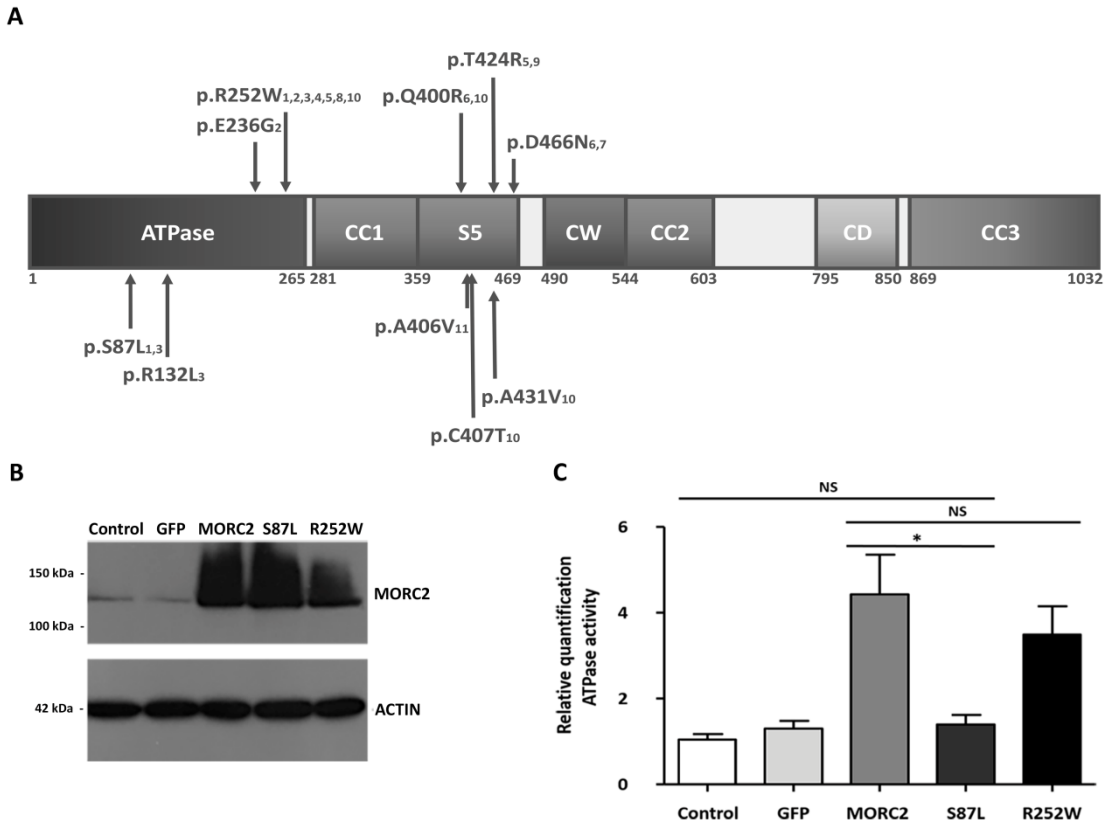

Figure 4. The level of ATPase activity in HeLa cells expressing wild-type and mutated forms of MORC2. **(A)** Schematic representation of MORC2 protein structure with the localization of mutations identified in CMT2Z patients. CC1, 2 and 3: coiled-coil domains; S5: ribosomal protein S5 domain; CW: CW-type finger domain; CD: Chromo-like domain. $_{1}$Sevilla et al., 2016 [4]; $_{2}$Albulym et al., 2016 [5]; $_{3}$Hyun et al., 2016 [8]; $_{4}$Lassuthova et al.,2016 [6]; $_{5}$Schottmann et al., 2016 [10]; $_{6}$Zhao et al., 2016 [7]; $_{7}$Semplicini et al., 2017 [11]; $_{8}$Bansagi et al., 2017 [9]; $_{9}$Zanni et al., 2017 [12]; $_{10}$Ando et al., 2017 [13]; $_{11}$Frasquet et al., 2018 [23]. **(B)** Western-blot demonstrating the relative level of MORC2 protein expression in HeLa cells transfected with the different isoforms of MORC2 and transduction controls. **(C)** ATPase assay in HeLa cells transduced with expression constructs for GFP and the different isoforms of MORC2. The enzymatic activity (U/mL) was normalized to the control [Activity ATPase Control = 1]. *=P <0.05, NS=Not significant.

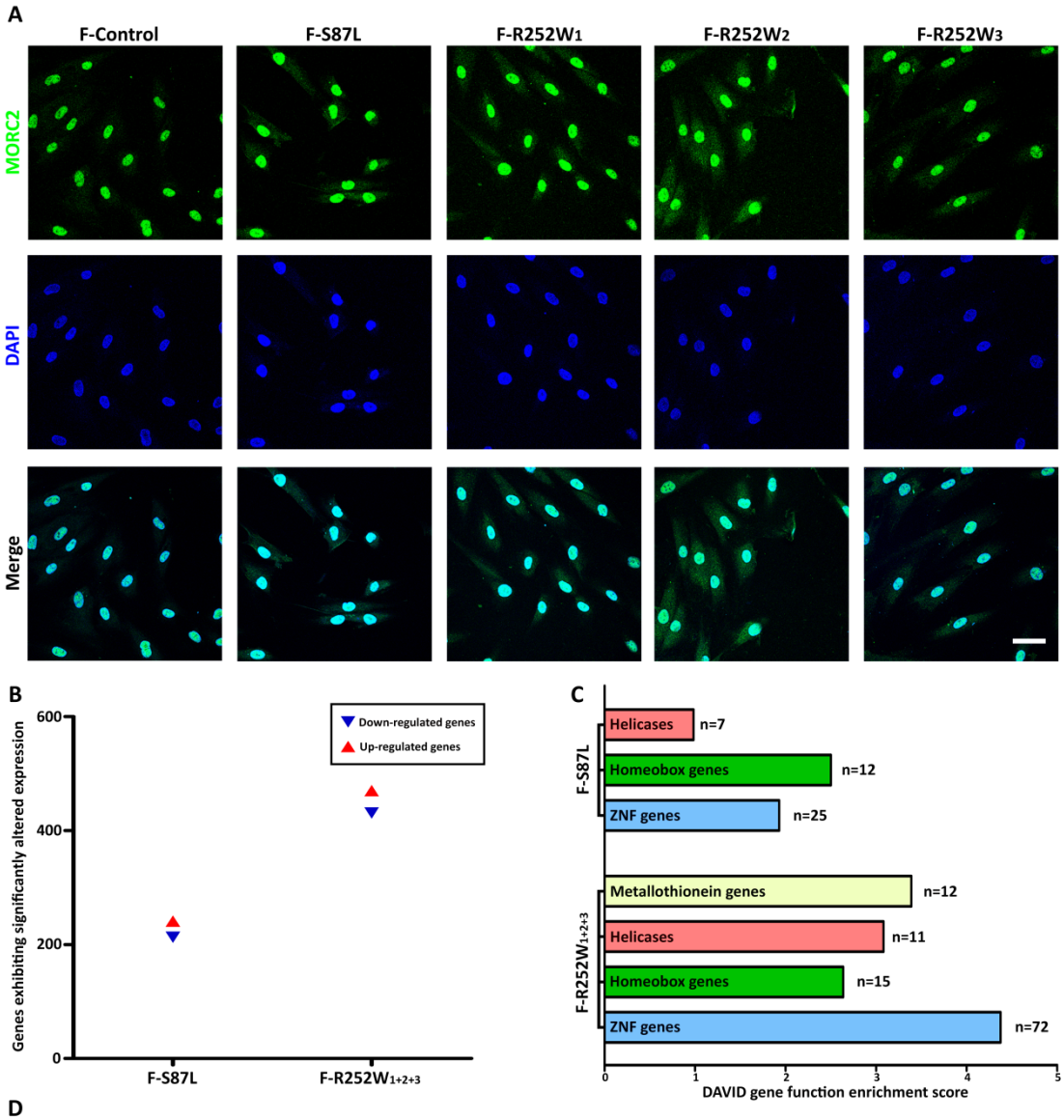

D

Repressed ZNF genes in F-S87L		
Gene name	Log fold change	Adj. p_value
ZNF454	-2.7814	0,0030
ZNF75A	-1.0237	0,0040
ZNF528	-1.3250	0,0169
ZNF540	-2.2426	0,0210
ZNF846	-1.2658	0,0210
ZNF502	-0.5908	0,0218
ZNF415	-2.6290	0,0241
ZNF594	-1.0206	0,0261
ZNF154	-1.4553	0,0261
ZNF157	-1.3509	0,0261
ZNF135	-1.7224	0,0310
SP9	-1.9272	0,0325
ZNF600	-0.9082	0,0325
ZNF132	-0.9453	0,0446
ZNF610	-1.3639	0,0446
ZNF575	-0.9276	0,0446

Repressed ZNF genes in F-R252W1+2+3					
Gene name	Log Fold change	Adj. p_value	Gene name	Log Fold change	Adj. p_value
ZNF594	-2.0444	0.0004	ZSCAN2	-0.4962	0.0172
ZNF454	-25782	0.0005	ZNF501	-0.4909	0.0172
ZNF717	-0.9719	0.0005	ZNF528	-0.8645	0.0172
ZNF518B	-0.8438	0.0006	ZNF600	-0.6658	0.0243
ZNF132	-1.2441	0.0013	ZSCAN18	-0.5705	0.0259
ZNF415	-2.3794	0.0076	ZFP64	-0.3451	0.0284
ZNF75A	-0.6543	0.0085	ZNF213	-0.8424	0.0288
ZNF425	-0.6632	0.0103	BNC1	-0.9917	0.0307
ZNF274	-0.6179	0.0106	ZNF584	-0.4787	0.0327
ZNF135	-1.5399	0.0106	ZNF79	-0.5056	0.0340
ZNF662	-1.2722	0.0107	SALL3	-0.4613	0.0355
ZNF793	-1.5777	0.0107	ZNF513	-0.5695	0.0379
ZBTB48	-0.6319	0.012	ZNF300	-0.8629	0.0389
BCL11A	-1.7346	0.012	ZNF787	-0.435	0.0390
SP9	-1.5631	0.016	ZNF630	-0.5834	0.0390
ZFP2	-0.8291	0.0169			

Figure 5. Characterization of human fibroblasts derived from CMT2Z patients carrying mutations S87L and R252W. **(A)** Immunofluorescence based analysis of MORC2 subcellular localization in fibroblast cultures. Scale bar=50 µM. **(B)** Number of genes

889 exhibiting significantly altered expression using a human fibroblast line derived from a
890 healthy subject as a control. Blue triangles are showing repressed genes and the red ones
891 indicate the over-expressed genes. **(C)** DAVID gene function enrichment score for the
892 patient fibroblast lines. **(D)** List of repressed *ZNF* genes for the patient fibroblast lines.
893 Genes in red were previously described to be regulated by MORC2 [21]. F-
894 Control=Fibroblast line derived from healthy control, F-S87L=Fibroblast line derived
895 from a patient carrying the p.S87L mutation, F-R252W=Fibroblast line derived from
896 patients carrying the p.R252W mutation (1, 2 or 3), F-R252W$_{1+2+3}$= average of
897 transcriptomic results obtained in three patients with MORC2 p.R252W mutation.
898
899
900
901
902
903
904
905
906
907
908
909
910
911
912
913

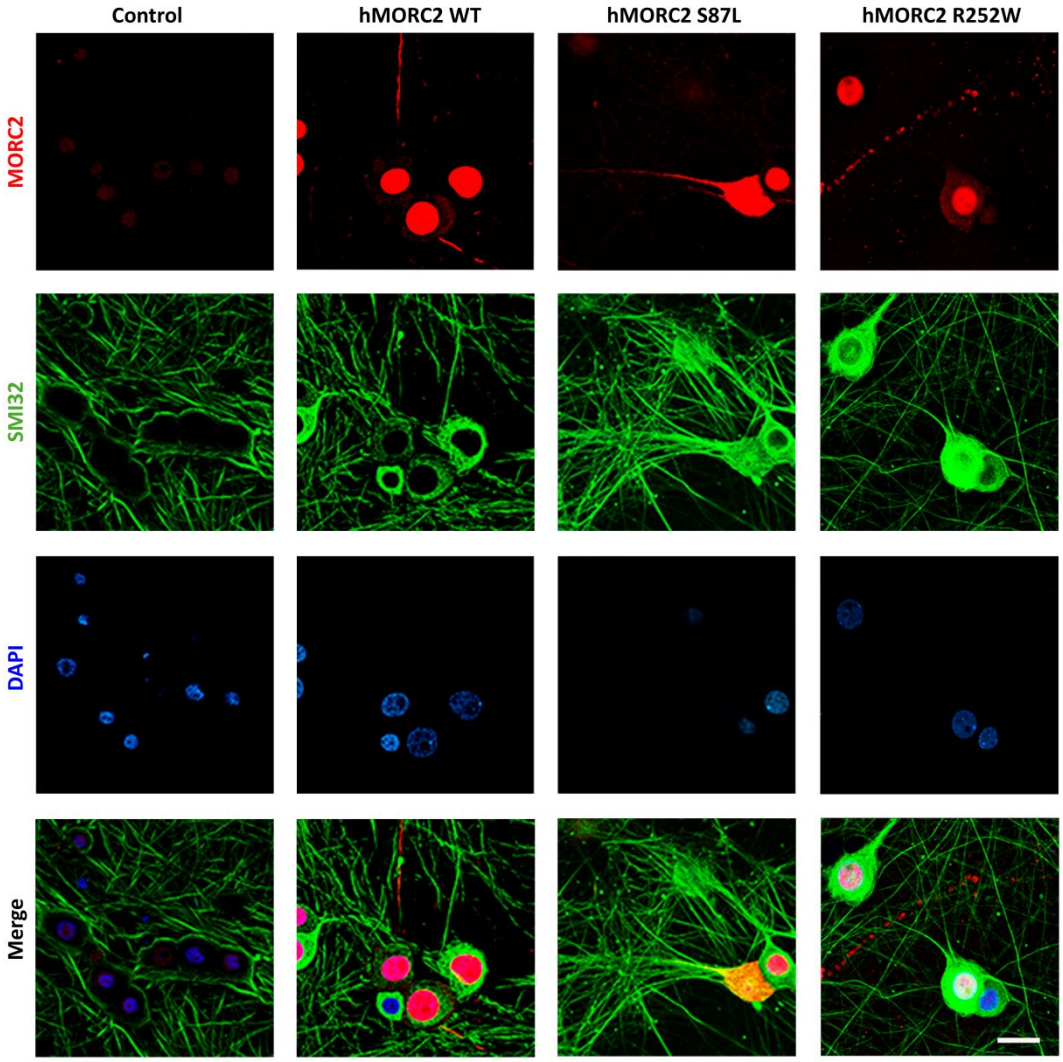

914

915 **Figure 6.** MORC2 expression in purified rat sensory neurons. Analysis of MORC2

916 subcellular localization in neuronal cultures infected with viruses carrying depicted

917 constructs. Virally mediated gene expression was induced for 4 days with doxycycline.

918 Scale bar=20 μM.

919

920

921

922

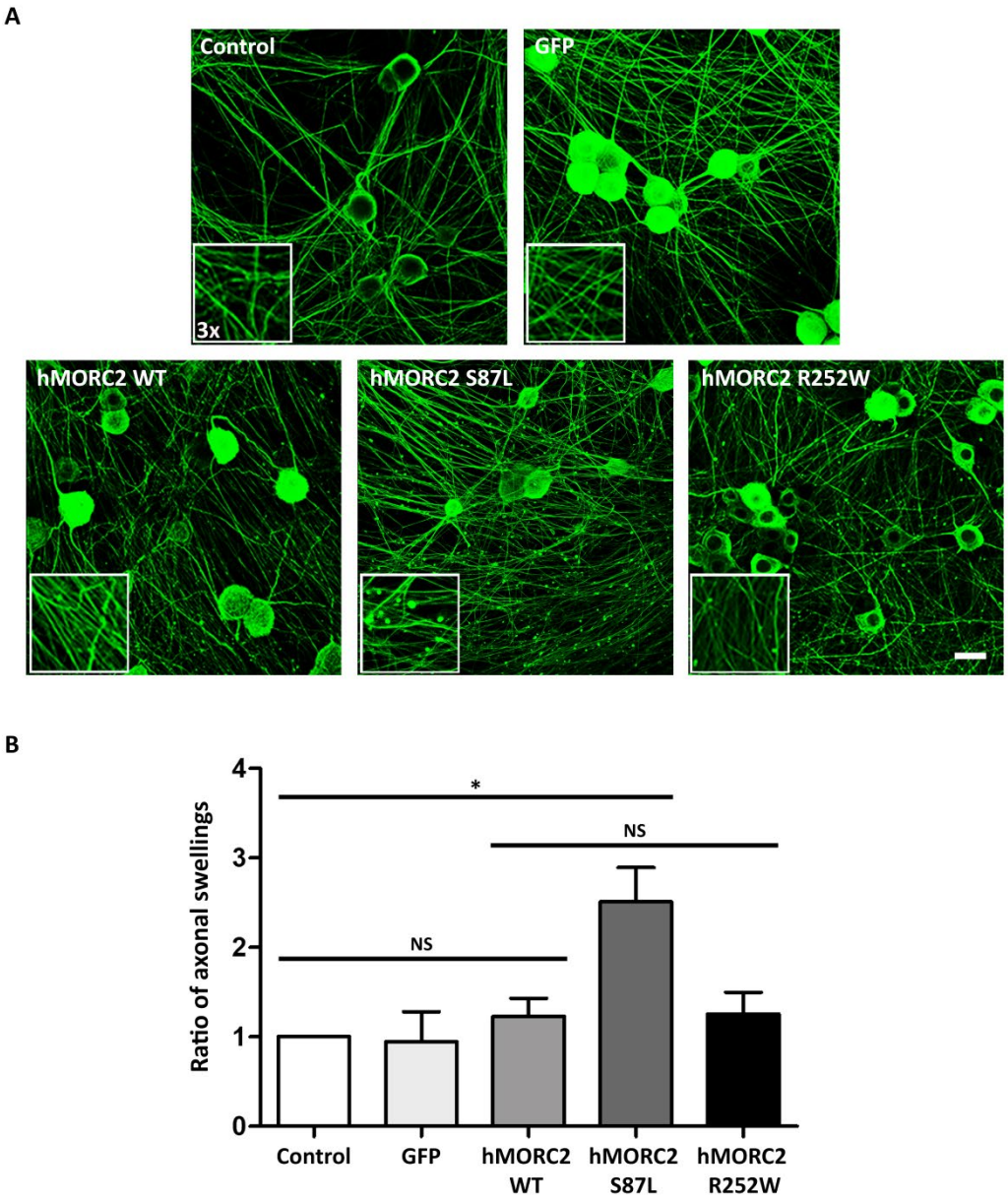

923

924 **Figure 7.** Analysis of axonal swellings induced by MORC2 expression in neuronal
925 cultures. **(A)** Neurofilament (SMI32) staining of infected neurons in which virally
926 mediated gene expression was induced for 4 days with doxycycline. Enlarged insets
927 (magnification 3x) are shown on bottom left of each image. Scale bar=20 μM. **(B)**
928 Quantification of axonal swellings. Number for uninfected (control) neuronal cultures
929 was set to 1 and all other values were appropriately normalized. *=P<0.05, NS=Not
930 significant.

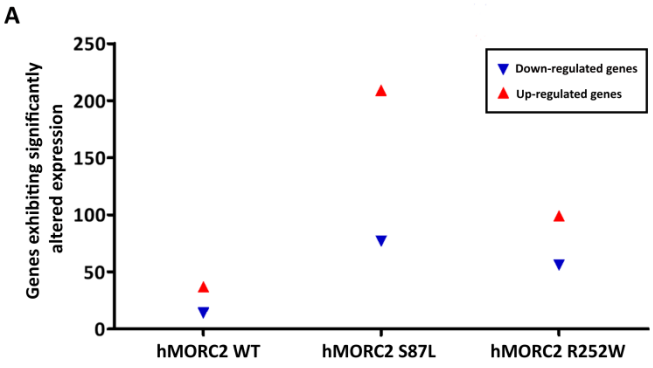

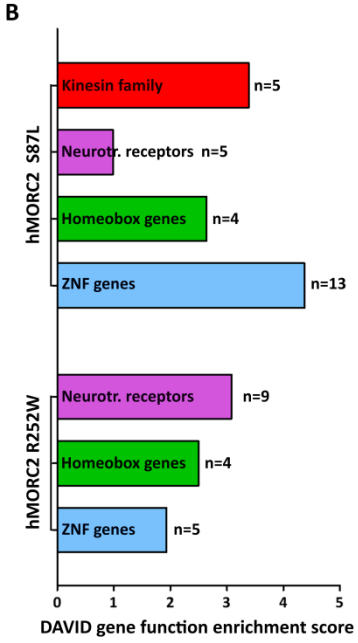

C

Altered neuronal-related genes in hMORC2 S87L			
Gene family	Gene name	Log fold change	Adj. p_value
AChE dinamycs-related	*Prima1*	-0.8107	0.0225
Chaperone-mediated protein folding	*Hspb1*	-2.0045	0.0138
Gaba receptors	*Gabra1*	1.8839	0.0102
	Gabra5	2.1599	0.0402
Glutamate receptors	*Grik3*	0.9542	0.0318
SLCs	*Slco3a1*	1.1453	0.0118
Kinesin family	*Kif18b*	2.6480	0.0012
	Kif20b	2.5508	0.0138
	Kifc1	1.4901	0.0103
	Kif20a	1.6522	0.0179
	Kif11	2.1956	0.0018

Altered neuronal-related genes in hMORC2 R252W			
Gene family	Gene name	Log fold change	Adj. p_value
Chaperone-mediated protein folding	*Hspb1*	-2.1645	0.0161
Gaba receptors	*Gabra1*	1.4898	0.0439
	Gabra5	2.4493	0.0306
	Gabrb1	2.4636	0.0322
Glutamate receptors	*Grik3*	1.0610	0.0292
nAChRs superfamily	*Chrnb4*	1.3944	0.0322
SLCs	*Slco3a1*	1.1645	0.0161
	Slc39a6	-0.6013	0.0475
TMEM proteins	*Tmem178a*	1.1397	0.0322
	Tmem81	-1.3848	0.0292

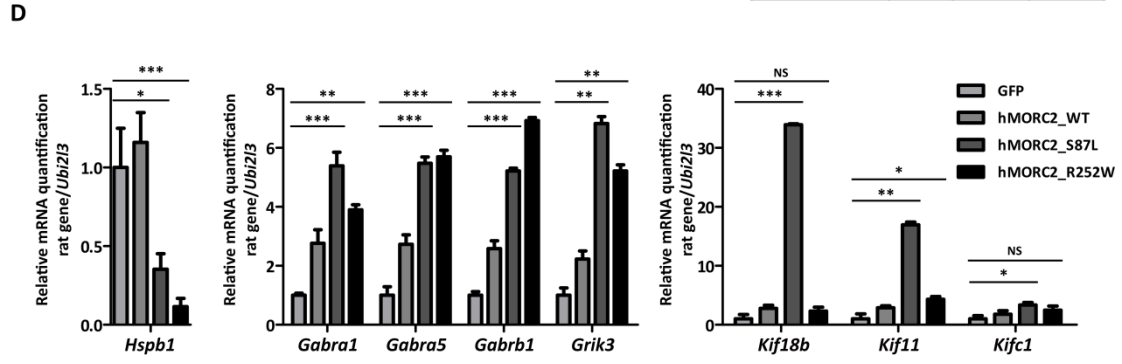

931

932 **Figure 8.** Transcriptional changes in sensory neurons expressing mutated forms of

933 Morc2. **(A)** Number of genes exhibiting significantly altered expression using GFP as a

934 control. Blue triangles are showing repressed genes and the red ones indicate the over-

935 expressed genes. **(B)** DAVID gene function enrichment score for the rat sensory
936 neurons expressing hMORC2 S87L and R252W. **(C)** Changes in genes encoding
937 proteins with recognized neuronal functions. **(D)** Quantitative-PCR based confirmation
938 of alterations found in the rat transcriptomic analysis. Ubiquitin (*Ubi2l3*) was used as
939 the normalizer for the amount of RNA used. The measurements obtained for GFP were
940 set as 1 and all other samples were appropriately normalized. *=P<0.05, **=P<0.001,
941 ***=P<0.0001, NS=Not significant.
942

943 **SUPPLEMENTARY MATERIAL**

944 **Figure S1.** Evaluation of primer efficiency. PCR amplifications on samples derived
945 from HeLa **(A)** and SH-SY5Y **(B)** cells to confirm the amplification efficiency of all
946 primer pairs. GAPDH primers were used as positive control. Neg.= samples without
947 template were used as a negative control.

948

949 **Figure S2.** Malate dehydrogenase activity in CMT2Z fibroblast. Enzymatic activity of
950 ACLY using the coupled MDH method. Histograms show the enzyme activity of MDH
951 in control fibroblasts and fibroblasts of a patient with the p.R252W mutation. The
952 results are represented as the mean ± SEM for three independent experiments.

953

954 **Figure S3.** Subcellular localization of MORC2 in HeLa cells. HeLa cells were infected
955 with depicted lentiviral vectors or kept uninfected (control). MORC2 is present mainly
956 in cellular nuclei, except for dividing cells where it is present in the cytoplasmic area.
957 Scale bar=50 μM.

958

959 **Figure S4.** Percentage of infected rat sensory neurons. The percentage of infected
960 neurons appeared unchanged using the four different lentiviral constructs. In the cells
961 infected with GFP, the positive GFP cells were counted. In the cells infected with
962 different constructs of MORC2, the nuclei stained with MORC2 were counted.

963

964 **Figure S5.** MORC2 expression in purified rat sensory neurons. **(A)** Analysis of
965 MORC2 expression by qPCR using RNA extracted from infected neurons. hMORC2
966 1F/R primers were used to detect *Morc2* expression and Ubiquitin (*Ubi2l3*) was used as
967 a normalizer. Data obtained from neurons expressing wild-type *Morc2* were set to 1 and

all other results were appropriately normalized. **(B)** MORC2 expression in control neurons, neurons infected with GFP and neurons infected with the different MORC2 constructs were analyzed by western-blot. Actin was used to validate equal protein loading. **(C)** Global view of control and infected neuronal cultures. In control and GFP conditions there are no nuclei overexpressing MORC2. 10x amplification. Scale bar=150 µM.

Figure S6. Subcellular localization of MORC2 in primary rat Schwann cells. Schwann cells were transfected with plasmids containing wild-type and mutated forms of *Morc2* or GFP as control. MORC2 is present mainly in cellular nuclei, except for the control transfection, where MORC2 expression was undetectable. Scale bar=20 µM.

Table S1. Genes differentially expressed between MORC2 and GFP.

Table S2. Genes differentially expressed between S87L and GFP.

Table S3. Genes differentially expressed between R252W and GFP.

Table S4. Genes related to inherited peripheral neuropathies.

Table S5. Altered ZNF genes.

990 **Table S6.** Altered homeobox genes.

991

992 **Table S7.** Primers sequences.

993

994 **Table S8.** RNA integrity for transcriptomic assays.

995

ABBREVIATIONS

AC: actin

ACLY: ATP-citrate lyase

ACRF: Australian Cancer Research Foundation

BSA: bovine serum albumin

CC1, 2 and 3: coiled-coil domains

CD: chromo-like domain

CMT: Charcot-Marie-Tooth

CMT2A2: Charcot-Marie-Tooth type 2A2

CMT2E: Charcot-Marie-Tooth type 2E

CMT2F: Charcot-Marie-Tooth type 2F

CMT2Z: Charcot-Marie-Tooth type 2Z

CW: CW-type finger domain

dHMN: distal hereditary motor neuropathy

dHMN2B: distal hereditary motor neuropathy type IIB

DMEM: Dulbecco's Modified Eagle's Medium

DRG: dorsal root ganglia

DTT: DL-Dithiothreitol

E: embryonic stage

1015 FBS: Fetal Bovine Serum

1016 FCS: fetal calf serum

1017 GABA: gamma-aminobutyric acid

1018 GFP: green fluorescent protein

1019 GHL: Gyrase B, Hsp90, and MutL

1020 HRP: horseradish peroxidase

1021 HUSH: human silencing hub

1022 MDH: malate dehydrogenase

1023 M: months

1024 MORC: microrchidia

1025 MORC2: microrchidia family CW-type zinc finger 2

1026 NB: neurobasal

1027 NBB: Netherlands Brain Bank

1028 NDRI: National Disease Research Interchange

1029 NFL: neurofilament light

1030 NGF: Nerve Growth Factor

1031 NGS: normal goat serum

1032 NS: not significant

1033 o/n: overnight

PBS: phosphate-buffered saline

P: post-natal day

P/S: Penicillin/Streptomycin

PAGE: polyacrylamide gel electrophoresis

PAK1: p21-activated kinase 1

PVDF: polyvinylidene difluoride

qPCR: quantitative-PCR

RT: room temperature

RT-PCR: real time PCR

S5: ribosomal protein S5 domain

SDS: sodium dodecyl sulfate

SEM: standard error of the mean

SMA: spinal muscular atrophy

WT: wild-type

Y: years

ZNF: zinc finger